

# SnO<sub>2</sub> Quantum Dots Functionalized 3D Graphene Composite for Enhanced Performance of Electrochemical Myoglobin Biosensor

Ying Deng<sup>1</sup>, Zuorui Wen<sup>1</sup>, Hui Cheng<sup>2</sup>, Lijun Yan<sup>1</sup>, Bo Shao<sup>1</sup>, Guangjiu Li<sup>2</sup>, Xiaoping Zhang<sup>1,\*</sup>, Wei Sun<sup>1,\*</sup>

<sup>1</sup> Key Laboratory of Laser Technology and Optoelectronic Functional Materials of Hainan Province, Key Laboratory of Functional Materials and Photoelectrochemistry of Haikou, College of Chemistry and Chemical Engineering, Hainan Normal University, Haikou 571158, P R China

<sup>2</sup> Key Laboratory of Optic-electric Sensing and Analytical Chemistry for Life Science of Ministry of Education, Shandong Key Laboratory of Biochemical Analysis, College of Chemistry and Molecular Engineering, Qingdao University of Science and Technology, Qingdao, P. R. China.

\*E-mail: [254787885@qq.com](mailto:254787885@qq.com) and [sunwei@hainnu.edu.cn](mailto:sunwei@hainnu.edu.cn)

Received: 26 June 2020 / Accepted: 3 August 2020 / Published: 30 August 2020

In this work, we reported on the electrochemical behaviors and electrocatalysis of myoglobin (Mb) biosensor based on SnO<sub>2</sub> quantum dots functionalized three-dimensional graphene composite (SnO<sub>2</sub>-QDs@3DGR) modified carbon ionic liquid electrode (CILE). The SnO<sub>2</sub>-QDs@3DGR composite was synthesized via a facile one-step hydrothermal strategy, which offered rich channels, enough active sites, high conductivity and good biocompatibility for bonding with Mb. The direct electron transfer (DET) performance between Mb and SnO<sub>2</sub>-QDs@3DGR modified electrode was greatly improved with electrochemical responses increased. In cyclic voltammetric investigation, a pair of well-defined redox peaks of Mb were observed with the formal peak potential of -0.263 V (E<sup>0</sup>) and a peak-to-peak separation of 75 mV (ΔE<sub>p</sub>). The heterogeneous electron transfer constant (k<sub>s</sub>) was calculated as 1.34 s<sup>-1</sup>. Furthermore, the modified electrode with chitosan (CTS) film (CTS/Mb/SnO<sub>2</sub>-QDs@3DGR/CILE) was used for the electrocatalysis of trichloroacetic acid, which showed a wider linear response from 5.0 to 94.0 mmol L<sup>-1</sup> with the limit of detection as 0.35 mmol L<sup>-1</sup>.

**Keywords:** 3D graphene · SnO<sub>2</sub> quantum dots · Direct electrochemistry · electrocatalysis · trichloroacetic acid

## 1. INTRODUCTION

Due to excellent properties inherited from two-dimensional graphene nanosheet including high conductivity, excellent mechanical property, and so on, three-dimensional graphene (3D-GR) has been recognized as a promising material, which has been applied in sensor, energy storage and conversion,

electrode material and environment treatment [1-5]. To further enhance the properties of 3D-GR, a variety of functional materials including polymers, metals, metal oxides with diverse structures have been introduced into the network of 3D-GR. Therefore, a series of synthesis strategies such as hydrothermal method, CVD method, template method and polymer crosslinking method etc., have been employed to construct various 3D-GR based hybrid materials [6-8]. Compared with their related single-species, the 3D-GR based hybrid materials commonly demonstrate dramatically enhanced electrochemical performance, which may be contributed to the unique 3D hybrid structure that can provide enough channels for efficient transportation of electrolyte and conductive networks for smoothly electron transfer.

Tin dioxide ( $\text{SnO}_2$ ) is an important metal oxide semiconductor with wide-band gap (3.6-4.0 eV), large surface area, nontoxicity, good biocompatibility, catalytic activity and chemical stability, which has been investigated for various applications such as solar cells, electrochemistry sensors and biosensors [9-12]. However, high operation temperature and agglomeration during synthesis with low conductivity have hitherto stifled more extensive applications. To overcome this limitation,  $\text{SnO}_2$  can be coupled with highly conductive material to get the nanocomposite. Kafi et al. reported on a glucose biosensor based on co-immobilization of glucose oxidase and horseradish peroxidase with polymerized multi-porous nanofiber  $\text{SnO}_2$  onto glassy carbon electrode (GCE) with chitosan (CTS) [13]. Zhou et al. fabricated an amperometric acetylcholinesterase biosensor based on  $\text{SnO}_2$  nanoparticles, carboxylic graphene and Nafion modified GCE for the detection of methyl parathion [14]. Thus,  $\text{SnO}_2$  is an excellent candidate for the synthesis of hybrid materials that can be applied to the field of sensing research.

Direct electron transfer (DET) between redox protein and electrode can not only explore the mechanism of proteins in the field of life science, but also provide guidance for enzyme catalysis, which has been recognized as the key of third-generation electrochemical biosensors with more attentions in recent years [15,16]. Among the reported redox proteins, myoglobin (Mb) is considered as an ideal model molecule for the DET of protein due to its well-known structure and commercial availability. But the DET process of Mb cannot be easily realized on the bare electrode because of the aggregation and unfavorable orientation of Mb that deeply buried of the electroactive center on the electrode surface. Therefore various modifiers or mediators have been used to accelerate the DET of Mb with direct electrochemistry realized [17-21]. In this work, a novel 3D network was successfully constructed by using porous 3D-GR as frameworks and  $\text{SnO}_2$  quantum dots ( $\text{SnO}_2$ -QDs) as insertion, which could provide rich pores and open channels with different size for the diffusion of electrolyte and enlarging the active surface area of Mb molecule. Finally, the as-fabricated biosensor (CTS/Mb/ $\text{SnO}_2$ -QDs@3DGR/CILE) demonstrated an enhanced DET process with excellent electrochemical response and outstanding electrocatalytic ability towards the reduction of trichloroacetic acid (TCA).

## 2. EXPERIMENTAL SECTION

### 2.1. Reagents

All electrochemical experiments were carried out with a CHI 660D electrochemical workstation (Shanghai CH Instrument, China) equipped with an electrochemical cell. A conventional three-electrode model were used with CTS/Mb/SnO<sub>2</sub>-QDs@3DGR/CILE as the working electrode, a platinum wire and saturated calomel electrode as auxiliary and reference electrodes, respectively. SEM and TEM images were obtained on JSM-7100F and JEM-2010F instruments (JEOL, Japan). X-ray diffraction (XRD) measurements were performed on a D/Max-2500V X-ray diffractometer (Rigaku, Japan) with Cu-K $\alpha$  radiation ( $\lambda = 1.54178 \text{ \AA}$ ). Raman spectrum was obtained on a LabRAM HR system using 532 nm lasers (Horiba, France). X-ray photoelectron spectroscopy (XPS) was done on an AXIS HIS 165 spectrometer (Kratos Analytical, UK).

Ionic liquid 1-hexylpyridinium hexafluorophosphate (HPPF<sub>6</sub>, Lanzhou Yulu Fine Chem. Co., China), Mb (MW 17800, Sigma, USA), graphene oxide (GO, Shanxi Tanmei Technology Co., China), graphite powder ( $\varphi = 30 \text{ \mu m}$ , Shanghai Colloid Chem. Co., China), CTS (Dalian Xindie Ltd. Co., China), SnCl<sub>2</sub>•2H<sub>2</sub>O (Guangzhou Xingang Chem. Co., China), carbamide (Hubei Sanning Chem. Co. LTD., China) and TCA (Tianjin Kemiou Chem. Ltd. Co., China) were used directly. Medical facial peel (35% TCA, Shanghai EKEAR Bio. Tech. Ltd. Co., China) was selected as the real sample. The supporting electrolyte was 0.1 mol L<sup>-1</sup> phosphate buffer solution (PBS), which was kept oxygen free during experiments.

### 2.2. Preparation of SnO<sub>2</sub>-QDs@3DGR nanocomposite

SnCl<sub>2</sub>•2H<sub>2</sub>O (66 mg) and carbamide (54 mg) were added in 20 mL water, and stirred well to form an uniform and clear solution. Then, the mixture solution was dropwise added in a 10 mL GO suspension (3.6 mg mL<sup>-1</sup>, ultra-sonicated for 30 min) under continuous stirring (1 h). The resulted mixture was sealed into a 50 mL reaction vessel and heated at 180°C for 16 h. After cooled to room temperature, a cylindrical hydrogel was obtained, which was washed with distilled water and ethanol for three times successively. Subsequently, the products were dried in vacuum at 60°C for 10 h.

### 2.3. Fabrication of CTS/Mb/SnO<sub>2</sub>-QDs@3DGR/CILE

Layer coating method was used to prepare the modified electrode. Prior to modification, CILE was fabricated and smoothed according to the reference [22]. 8.0  $\mu\text{L}$  0.8 mg mL<sup>-1</sup> SnO<sub>2</sub>-QDs@3DGR suspension was dropped onto the CILE surface and left to dry at room temperature, then 12.0 mg mL<sup>-1</sup> Mb solution was casted on SnO<sub>2</sub>-QDs@3DGR/CILE surface. Finally, 5.0  $\mu\text{L}$  of CTS (1.0% HAC) was further decorated on the electrode to form a stable film and the resulted electrode was denoted as the working electrode (CTS/Mb/SnO<sub>2</sub>-QDs@3DGR/CILE). For comparison, other modified electrodes were fabricated similar to the proposed method.

### 3. RESULTS AND DISCUSSION

#### 3.1. Characterizations of nanocomposite

The XRD pattern of SnO<sub>2</sub>-QDs@3DGR is shown in Fig.1A. It is observed that wide peaks at 26.61° (110), 37.95° (200), 33.89° (101), 51.78° (211) in Fig. 1A are corresponding to a tetragonal rutile structure (JCPDS 41-1445). Fig. 1B displays the Raman spectrum of SnO<sub>2</sub>-QDs@3DGR with the peaks of D and G bands clearly observed at 1350 cm<sup>-1</sup> and 1850 cm<sup>-1</sup>. According to the intensity ratio of D to G bands (D/G=1.15), the SnO<sub>2</sub>-QDs@3DGR presents larger defect concentration that may cause by the presence of SnO<sub>2</sub> nanoparticles.

The XPS survey spectrum of SnO<sub>2</sub>-QDs@3DGR is recorded, which indicates that C, Sn, O elements are co-existed in the 3D composite structure (Fig.1C). The enlarged C 1s spectrum (Fig.1D) demonstrates that there are three bonding type of C element (C-C, C-O and C=O models), corresponding to the fitted peaks at 284.6 eV, 285.5 eV, and 288.7 eV, respectively. As shown in Fig. 1E, the strong peaks at 487.1 eV and 495.6 eV may ascribe to Sn 3d<sub>3/2</sub> and Sn 3d<sub>5/2</sub>, which further confirm the formation of SnO<sub>2</sub> nanoparticles [23]. In the O 1s region (Fig.1F), the peak at 531.4 eV is assigned to the lattice oxygen (O<sub>L</sub>) of Sn-O-Sn, the peak at 532.0 eV is assigned to the oxygen vacancy on the surface of SnO<sub>2</sub> QDs and GR, and the peak at 532.6 eV is assigned to the chemisorbed oxygen (O<sub>C</sub>) of O<sub>2</sub> or H<sub>2</sub>O.

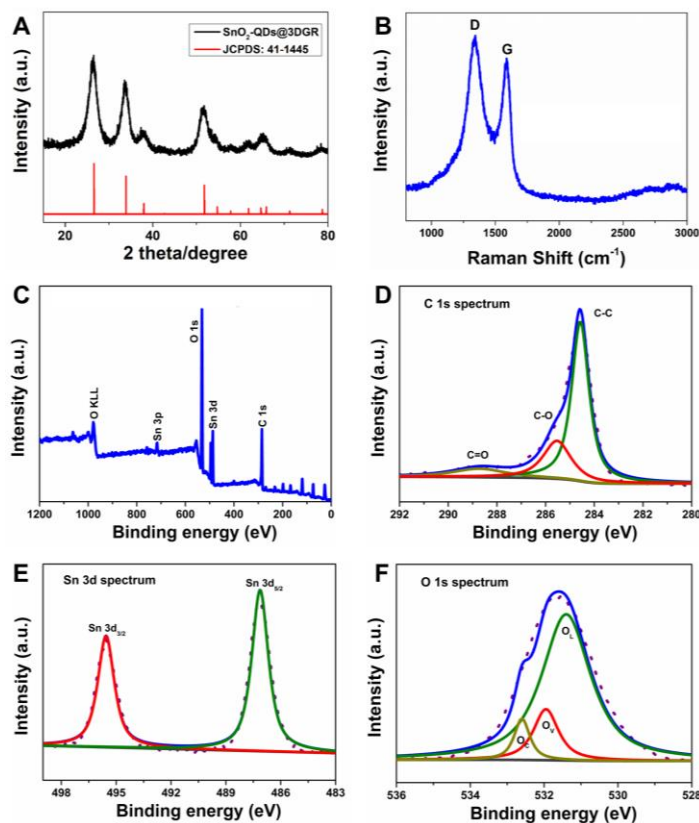


**Figure 1.** XRD (A) and Raman spectra (B) of SnO<sub>2</sub>-QDs@3DGR, XPS survey spectrum (C), and the C 1s (D), Sn 3d (E) and O 1s (F) XPS spectra of SnO<sub>2</sub>-QDs@3DGR

As shown in Fig.2A, the synthesized SnO<sub>2</sub>-QDs@3DGR by hydrothermal method appears as a cylindrical blocks. SEM images of SnO<sub>2</sub>-QDs@3DGR with different magnifications are shown in Fig. 2B and 2C. It is observed that SnO<sub>2</sub>-QDs@3DGR presents a 3D reticulated structure that constructed with wrinkled GR nanosheets. The loose 3D structure can provide abundant channels and smooth electronic transmission channels with different sizes, it can also enlarge the active surface area for binding protein molecule, which is supposed to enhance the DET performance and electrocatalytic ability. TEM image (Fig. 2D) displays that a series of SnO<sub>2</sub>-QDs are randomly distributed on the surface of GR nanosheets. The enlarged TEM demonstrates that the diameter of SnO<sub>2</sub>-QDs is in the range of 3-5 nm (Fig 2E). The interplanar spacing of 0.33 nm (Fig. 2F) is corresponding to the (110) planes of SnO<sub>2</sub> in the rutile phase, which is consisted with the XRD peaks. The unique 3D structure composite takes advantages of synergetic effects of SnO<sub>2</sub> and GR with high electron transfer efficiency and bio-compatibility for improving electrochemical performance.

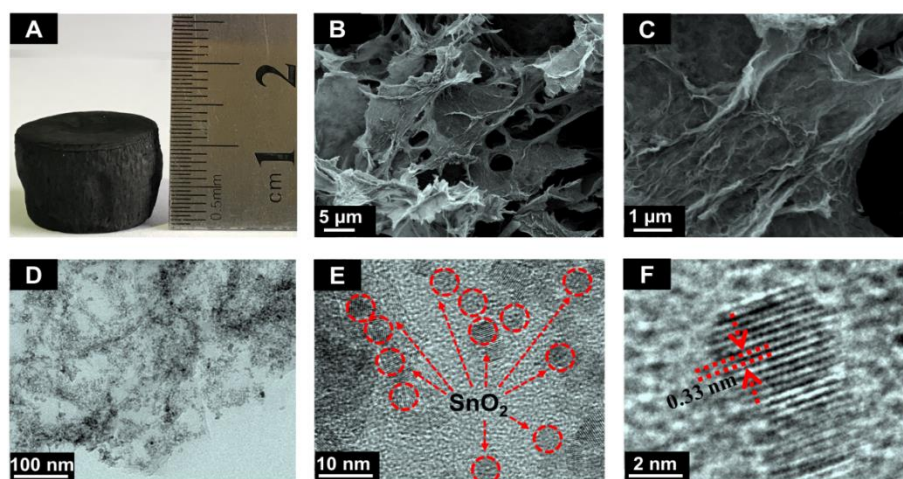


**Figure 2.** (A) The physical photograph, (B-C) SEM images, (D) TEM image and (E-F) HRTEM images of SnO<sub>2</sub>-QDs@3DGR at different magnification sizes.

### 3.2 Electrochemical properties

To investigate the effect of SnO<sub>2</sub>-QDs@3DGR on electrochemical signal of the modified electrode, cyclic voltammograms of different electrodes are measured in standard potassium ferricyanide solution at scan rate of 0.1 V s<sup>-1</sup> with the obtained curves shown in Fig. 3A. It can be seen that all electrodes possess a pair of redox peaks. However, in contrast to CILE (curve c) and CTS/Mb/CILE (curve d), the peak currents of CTS/SnO<sub>2</sub>-QDs@3DGR/CILE (curve a) and CTS/Mb/SnO<sub>2</sub>-QDs@3DGR/CILE (curve b) increase dramatically, which can be ascribed to the introduction of SnO<sub>2</sub>-QDs@3DGR nanocomposite that enhance the effective surface area. Meanwhile, the redox peak currents (*I<sub>p</sub>*) of modified electrode in the presence of macromolecule Mb (curve a) is reduced, which is obviously due to the biological macromolecules hampering the electron transfer.

Electrochemical impedance spectroscopy (EIS) is a method of feedback for effectively demonstrating impedance information of different electrodes, the resistance value (*R<sub>et</sub>*) can be obtained from the diameter of the impedance diagram semicircle. Fig. 3B illustrates the Nyquist plots of four

modified electrodes within the scan frequency from  $10^5$  to  $10^{-1}$  Hz in a  $1.0 \text{ mmol L}^{-1}$   $[\text{Fe}(\text{CN})_6]^{3-/4-}$  and  $0.5 \text{ mol L}^{-1}$  KCl solution. As expected, the bare electrode only covered with CTS membrane (curve c) shows semicircle diameter with  $R_{\text{et}}$  as  $50.32 \Omega$ . After modification with the  $\text{SnO}_2\text{-QDs@3DGR}$ , the  $R_{\text{et}}$  of the modified electrode (curve a) decreases to  $17.28 \Omega$ . This result is mainly because of three-dimensional network structure of hybrid nanomaterial, which reduces the electron bond. However, the presence of biomolecules makes the resistance even greater, as seen from the  $R_{\text{et}}$  values of CTS/Mb/ $\text{SnO}_2\text{-QDs@3DGR/CILE}$  (curve b) and CTS/Mb/CILE (curve d). In addition, it can be notably observed that the  $R_{\text{et}}$  of CTS/Mb/ $\text{SnO}_2\text{-QDs@3DGR/CILE}$  is smaller than that of CTS/Mb/CILE, which confirms that  $\text{SnO}_2$  quantum dot and graphene network-like material decrease the interfacial resistance.

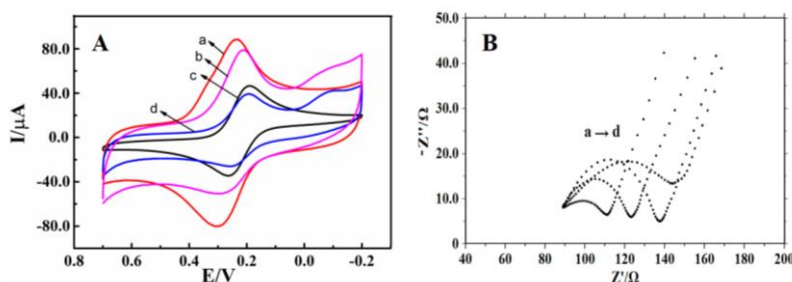


**Figure 3.** (A) Cyclic voltammograms of (a) CTS/ $\text{SnO}_2\text{-QDs@3DGR/CILE}$ , (b) CTS/Mb/ $\text{SnO}_2\text{-QDs@3DGR/CILE}$ , (c) CILE, (d) CTS/Mb/CILE in  $1.0 \text{ mmol L}^{-1}$   $[\text{Fe}(\text{CN})_6]^{3-/4-}$  solution containing  $0.5 \text{ mol L}^{-1}$  KCl, Scan rate:  $100 \text{ mV s}^{-1}$ . (B) Electrochemical impedance spectra of (a) CTS/ $\text{SnO}_2\text{-QDs@3DGR/CILE}$ , (b) CTS/Mb/ $\text{SnO}_2\text{-QDs@3DGR/CILE}$ , (c) CTS/CILE, (d) CTS/Mb/CILE in a solution of  $5.0 \text{ mmol L}^{-1}$   $[\text{Fe}(\text{CN})_6]^{3-/4-}$  and  $0.1 \text{ mol L}^{-1}$  KCl with the frequencies swept from  $10^5$  to  $10^{-1}$  Hz.

### 3.3 Electrochemical behavior of Mb at different modified electrodes

The effective redox activity site of Mb is acknowledged as the co-factor heme group  $[\text{Fe}(\text{II})/\text{Fe}(\text{III})]$  and is responsible for its direct electrochemical behavior on the electrode surface. Herein, the electrochemical behaviors of Mb immobilized at the surface of different modified electrodes are carried out in  $\text{N}_2$ -saturated pH 5.0 PBS with scan rate of  $100 \text{ mV s}^{-1}$  under the electrochemical window between  $-0.6$  and  $0.2 \text{ V}$ . As shown in Fig. 4, no peaks are observed at three modified electrodes (curve c to e), indicating that there is no redox reaction under this potential window due to the absence of Mb. In addition, the modification of  $\text{SnO}_2\text{-QDs@3DGR}$  (curve c) lead to the broader background currents. As for CTS/Mb/CILE (curve b), a pair of redox peaks are observed, demonstrating the realization of DET of Mb with the electrode. While on CTS/Mb/ $\text{SnO}_2\text{-QDs@3DGR/CILE}$  (curve a), the symmetrical redox peaks appeared with increased peak currents. The peak potentials are located at  $-0.304 \text{ V}$  ( $E_{\text{pa}}$ ) and  $-0.220 \text{ V}$  ( $E_{\text{pc}}$ ) with a peak-to-peak separation ( $\Delta E_{\text{p}}$ ) of  $75 \text{ mV}$ . The result indicates that  $\text{SnO}_2\text{-QDs@3DGR}$  nanocomposite material with large specific surface area and excellent conductive performance provides more attachment sites for the immobilization of Mb and such a suitable microenvironment is benefit for effective electron transfer.

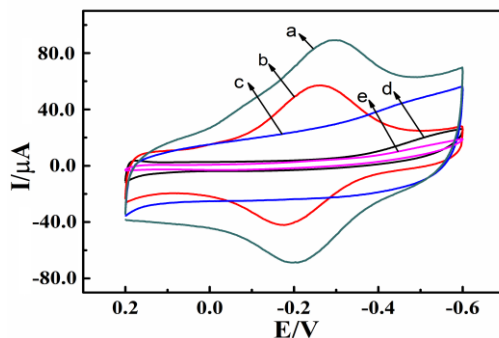


**Figure 4.** Cyclic voltammograms of (a) CTS/Mb/SnO<sub>2</sub>-QDs@3DGR/CILE, (b) CTS/Mb/CILE, (c) CTS/SnO<sub>2</sub>-QDs@3DGR/CILE, (d) CTS/CILE, (e) CILE in pH 5.0 PBS with the scan rate as 100 mV s<sup>-1</sup>.

### 3.4 Effect of scan rate

Cyclic voltammograms of CTS/Mb/SnO<sub>2</sub>-QDs@3DGR/CILE are recorded at varying scan rates from 20 to 800 mV s<sup>-1</sup> for understanding the electron transfer characteristics of Mb with the result shown in Fig.5A. All cyclic voltammetric curves have a pair of well-defined quasi-reversible peaks, and the redox peak currents of Mb increase gradually with scan rate with the corresponding potentials showing a greater degree of positive and negative shift. The plots of scan rate vs. peak current of Mb are constructed and the results are shown in Fig. 5B. It can be seen that the anodic and cathodic redox peak current of Mb have a linear dependence on scan rate, indicating that an adsorption control process dominates the whole cyclic voltammetric scanning process. The linear regression equations are expressed as  $I_{pc}(\mu A) = 254.14v (V s^{-1}) + 12.031$  ( $n = 11, \gamma = 0.996$ ) and  $I_{pa}(\mu A) = -118.15v (V s^{-1}) - 7.431$  ( $n = 11, \gamma = 0.996$ ). The surface covering concentration of enzyme electroactive substances ( $\Gamma^*$ , mol cm<sup>-2</sup>) can be calculated as  $2.37 \times 10^{-9}$  mol cm<sup>-2</sup> in accordance with equation ( $Q = nF\Gamma^*$ ) [24], which exceeds the theoretical monolayer surface concentration ( $1.89 \times 10^{-11}$  mol cm<sup>-2</sup>) [25] for two orders of magnitude. It can be concluded that more proteins can be absorbed by multiple channels with a rough network surface of SnO<sub>2</sub>-QDs@3DGR.

Fig.5C shows this cyclic voltammetric process is a quasi-reversible electrochemical process with the linear fitting equation of  $E_{pa} (V) = 0.018 \ln v (V s^{-1}) - 0.23$  ( $\gamma = 0.998$ ) and  $E_{pc} (V) = -0.032 \ln v (V s^{-1}) - 0.37$  ( $\gamma = 0.999$ ). According to Laviron's equation [26], the values of the electron transfer coefficient ( $\alpha$ ) and the electron transfer number ( $n$ ) are 0.58 and 1.2, respectively. The apparent heterogeneous electron transfer rate constant ( $k_s$ ) are calculated as 1.34 s<sup>-1</sup>, which is superior to those reported in other papers [27-29]. The result demonstrates the improving kinetic process that the interaction of SnO<sub>2</sub>-QDs@3DGR with the active sites of Mb facilitates the electron transfer.

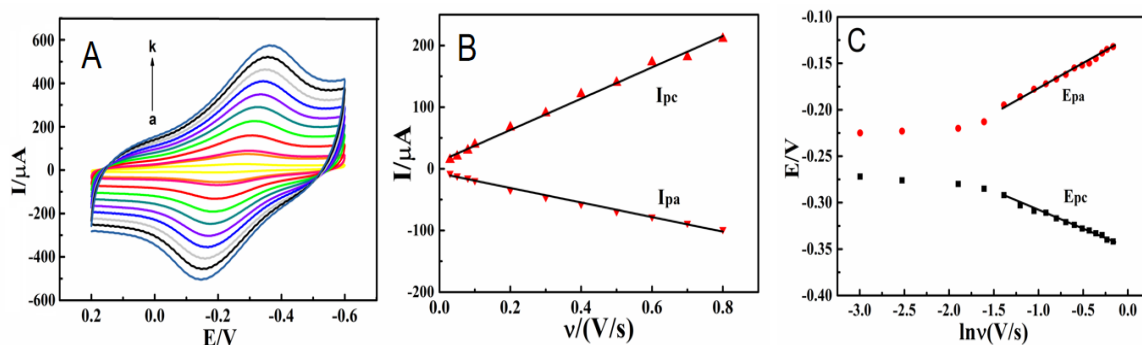


**Figure 5.** (A) Cyclic voltammograms of CTS/Mb/SnO<sub>2</sub>-QDs@3DGR/CILE at different scan rates (a-k: 20, 50, 80, 100, 200, 300, 400, 500, 600, 700, 800 mV s<sup>-1</sup>) in PBS; (B) Linear relationships of the redox peak currents vs. scan rate ( $v$ ); (C) Linear relationships of the redox peak potentials vs.  $\ln v$ .

### 3.5 Electrocatalytic activity

TCA is a kind of commonly used chemical in the fields of production and life, which has toxic effects on plants and human health. Therefore, it is necessary to develop a convenient detection method for TCA analysis. Herein, the prepared CTS/Mb/SnO<sub>2</sub>-QDs@3DGR/CILE is used for TCA detection. As shown in Fig. 6, continuously injection of a certain quantification of TCA into PBS results in a very fast current response. The cathodic peak current at -0.552 V is gradually increased with the TCA concentration changing from 5.0 to 94.0 mmol L<sup>-1</sup>, which is consisted with the typical TCA electrocatalysis reduction. In the process, Mb Fe(III) loses an electron to form Mb Fe(II), which catalyzes the dechlorination of TCA, and then Mb Fe(I) will be produced due to the further reduction of Mb Fe(II). The linear relationship of peak current and TCA concentration is obtained as  $I_{pc} (\mu A) = 4.04 C (\text{mmol L}^{-1}) + 12.2$  ( $n=18$ ,  $\gamma = 0.989$ ) with detection limit of 0.35 mmol L<sup>-1</sup> ( $3\sigma$ ). A typical Michaelis-Menten kinetic process appeared because that the  $I_{pc}$  reaches a limit value when the TCA concentration exceeds 94.0 mmol L<sup>-1</sup>. Based on the Lineweaver-Burk equation:

$$\frac{1}{I_{SS}} = \frac{1}{I_{max}} + \frac{K_M^{app}}{I_{max}C}$$

$I_{SS}$  is steady state current after addition of substrate,  $C$  is the volume concentration of substrates,  $I_{max}$  is the maximum current under the saturated state of the substrate. Consequently, the apparent Michaelis-Menten constant ( $K_M^{app}$ ) is calculated as 2.5 mmol L<sup>-1</sup>, the lower  $K_M^{app}$  value also implies the obviously stronger interaction between Mb and substrate. The catalytic performances of enzyme sensors modified by different catalysts for TCA are presented in Table 1. It is found that the CTS/Mb/SnO<sub>2</sub>-QDs@3DGR/CILE displays wide detection range and low limit of detection (LOD) compared with other modified electrodes, which shows excellent electrochemical response and outstanding electrocatalytic ability towards the reduction of TCA due to the presence of the SnO<sub>2</sub>-QDs@3DGR SnO<sub>2</sub>-QDs@3DGR.

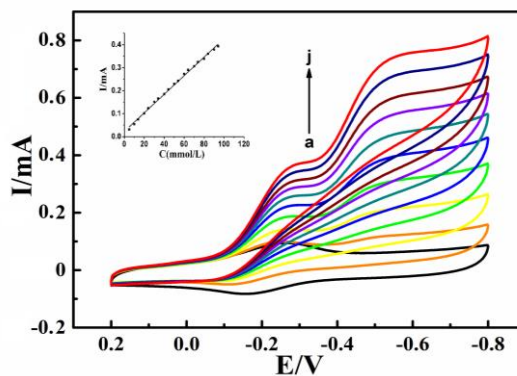


**Figure 6.** Cyclic voltammograms of CTS/Mb/SnO<sub>2</sub>-QDs@3DGR/CILE in the presence of different concentrations of TCA (from a to j as 5, 14, 24, 34, 44, 54, 64, 74, 84, 94 mmol L<sup>-1</sup>) with the scan rate as 100 mV s<sup>-1</sup>. Inset is the linear relationship of catalytic reduction peak currents and the TCA concentration.

**Table 1.** Catalytic performances of enzyme sensors modified by different catalysts for TCA

Modified electrode	$K_{Mapp}$ (mmol·L <sup>-1</sup> )	Limit of detection (mM)	Linear range (mM)	Ref.
Nafion/Mb-Co <sub>3</sub> O <sub>4</sub> -Au/IL-CPE	4.7	0.5	2.0-20.0	[21]
Nafion/Hb/Co <sub>3</sub> O <sub>4</sub> -CNF/CILE	/	1.33	4.0–260.0	[28]
Nafion/Hb-IL-GR-NiO/CILE	/	0.5	1.5–10.0	[29]
Mb/GR-Pt/CILE	0.126	0.32	0.9-9.0	[30]
Nafion-GO <sub>x</sub> -SWCNH	8.5	6	32-140	[31]
Nafion/HRP/WS <sub>2</sub> /CILE	4.5	0.4	5.0–27.0	[32]
CTS/ELDH-GR-Hb/CILE	7.93	1.506	5.0–360.0	[33]
CTS/Mb/SnO <sub>2</sub> -QDs@3DGR/CILE	2.5	0.35	5.0 - 94.0	This work

### 3.6 Application, Stability and reproducibility of CTS/Mb/SnO<sub>2</sub>-QDs@3DGR/CILE

The content of TCA in medical facial peel solution is detected by using CTS/Mb/SnO<sub>2</sub>-QDs@3DGR/CILE with the results displayed in Table 2. It can be seen that the recovery from 99.1% to 102.4% is obtained by using standard addition method and the relative standard deviation (RSD) is got from 1.5% to 2.8%. After storing for 30 days in a refrigerator, CTS/Mb/SnO<sub>2</sub>-QDs@3DGR/CILE displays high stability that their cyclic voltammetric curves exhibit small change (retain 93.4% of its initial value). The current responses of 12 electrodes are measured by adding 1.0 mmol L<sup>-1</sup> TCA to explore the reproducibility of CTS/Mb/SnO<sub>2</sub>-QDs@3DGR/CILE. The result shows a RSD value of 2.37 %, implying a good reproducibility.

**Table 2.** Analysis of TCA content in medical facial peel (n = 3)

Samples	Detected (mmol L <sup>-1</sup> )	Added (mmol L <sup>-1</sup> )	Total (mmol L <sup>-1</sup> )	Recovery (%)	RSD (%)
Medical		10.0	63.27	101.5	1.5
facial	52.32	20.0	72.95	102.4	2.3
peel solution		30.0	82.16	99.1	2.8

#### 4. CONCLUSIONS

Summary, an electrochemical biosensor composed of Mb and SnO<sub>2</sub>-QDs@3DGR was fabricated with enhanced electrochemical signal. SnO<sub>2</sub>-QDs@3DGR nanocomposite with three dimensional multi-channels was synthesized by a hydrothermal method and characterized by SEM, TEM, XPS, Raman methods. The biosensor demonstrated a fast direct electron transfer behavior and good electrocatalytic reduction toward TCA due to the synergistic effect among SnO<sub>2</sub>-QDs, 3DGR and Mb. DET process of Mb on the as-fabricated CTS/Mb/SnO<sub>2</sub>-QDs@3DGR/CILE was carefully investigated with the parameters calculated. Furthermore, this new sensor (CTS/Mb/SnO<sub>2</sub>-QDs@3DGR/CILE) had the characteristics of good stability, wide detection range and low LOD, which showed excellent performances in the analysis of TCA contents in real sample. Therefore, SnO<sub>2</sub>-QDs@3DGR is expected to be used in the construction of new electrochemical sensor and applied in the actual sample detection.

#### ACKNOWLEDGEMENTS

We acknowledge the financial support of Hainan Provincial Natural Science Foundation of High Level-talent Project (2019RC188), Open Project of Chemistry Department of Qingdao University of Science and Technology (QUSTHX201935), and Postgraduate innovative research of Hainan Normal University (Hsyx2018-9).

#### References

1. V. Chabot, D. Higgins, A. Yu, X. C. Xiao, Z. W. and Chen, J. J. Zhang, *Energ. Environ. Sci.*, 7 (2014) 1564.
2. X. Huang, Z. Y. Zeng, Z. X. Fan, J. Q. Liu, and H. Zhang, *Adv. Mater.*, 2445 (2012) 5979.
3. Y. Xia, P. Yang, Y. Sun, Y. Y. Wu, B. Mayers, B. D. Gates, Y. D. Yin, F. Kim, and H. Q. Yan, *Adv. Mater.*, 155 (2003) 353.
4. X. L. Niu, X. Y. Li, W. Chen, X. B. Li, W. J. Weng, C. X. Yin, R. X. Dong, W. Sun and G. J. Li, *Mat. Sci. Eng. C-Mater.*, 89 (2018) 230.
5. W. Sun, F. Hou, S. X. Gong, L. Han, W. C. Wang, F. Shi, J. W. Xi, X. L. Wang and G. J. Li, *Sens. Actuat. B-Chem.*, 219 (2015) 331.
6. S. Kabir, A. Serov, and P. Atanassov, *J. Power Sources*, 375 (2018) 255.
7. M. Loeblein, S. H. Tsang, M. P. Eric, J. R. Phua, H. Yong, X. Wu. Zhang, C. L. Gan, E. Hang, and T. Teo, *ACS Nano*.11 (2017) 2033..
8. F. Shi, J. W. Xi, F. Hou, L. Han, G. J. Li, S. X. Gong, C. X. Chen, and W Sun, *Mat. Sci. Eng. C-*

- Mater.*, 58 (2016) 450.
9. X. T. Yin, and T. Lin, *J. Alloy. Compd.*, 727 (2017) 254..
  10. A. A. Ensafi, and A. M. Rezaei, *Sens. Actuat. B-Chem.*, 296 (2019) 126683.
  11. W. Wang, Y. J. Zhu, and L.X. Yang, *Adv. Funct. Mater.*, 17 (2010) 59.
  12. W. Sun, X. Z. Wang, Y. H. Wang, X. M. Ju, L. Xu, G. J. Li and Z. F. Sun, *Electrochim. Acta*, 87 (2013) 317.
  13. S. Alim, A. K. M. Kafi, J. Rajan, and M. M. Yusoff, *Int. J. Biol. Macromol.*, 123 (2019) 1028.
  14. Q. Zhou, L. Yang, G. C. Wang, and Y. Yang, *Biosens. Bioelectron.*, 49 (2013) 25..
  15. W. Sun, L. L. Cao, Y. Deng, S. X. Gong, F. Shi, G. N. Li and Z. F. Sun, *Anal. Chim. Acta*, 781 (2013) 41.
  16. I. Taurino, G. Sanz , R. Antiochia, C. Tortolini, F. Mazzei, G. Favero, G. Micheli and S. Carrara, *Anal. Chem.*, 79 (2016) 151.
  17. X. Q. Chen, H. Q. Yan, W. Sun, G.Y. Chen, C. J. Yu, W. Feng and Q. Lin, *RSC Adv.* 8 (2018) 38003.
  18. C. Yu, H. Sun and S. F. Hou, *Anal. Methods*, 9 (2017) 4873.
  19. R. Y. Zou, X. B. Li, G. L. Luo, Y. Niu, W. J. Weng, W. Sun, J. W. Xi, Y. Chen, G. J. Li, *Electroanalysis*, 31 (2019) 575.
  20. Y. Y. Niu, H. Xie, G. L. Luo, W. J. Weng, C. X. Ruan, G. J. Li and W. Sun, *RSC Adv.*, 9 (2019) 4480.
  21. X. Q. Chen, H. Q. Yan, Z. F. Shi, Y. H. Feng, J. C. Li, Q. Lin, Wang, X. H. and W. Sun, *Polym. Bull.*, 74 (2017) 75.
  22. H. Xie, X. Y. Li, G. L. Luo, Y. Niu, R. Y. Zou, C. X. Yin, S. M. Huang, W. Sun and G. J. Li, *Diam. Relat. Mater.*, 97(2019) 107453.
  23. L. Zhang, H. Shi, Y. H. Huang, H. Y. Xu, K. W. Xu, P. K. Chu and F. Ma. *ACS Appl. Surf. Sci.*, 11 (2019) 12958.
  24. A. J. Bard, L. R. Faulkner, *Electrochemical Methods Fundamentals and Applications*, Wiley, New York, (1980) 459.
  25. S. F. Wang, T. Chen, Z. L. Zhang, X. C. Shen, Z. X. Lu, D. W. Pang and K. Y. Wong, *Langmuir*, 21 (2005) 9260.
  26. E. Laviron, *J. Electroanal. Chem.*, 101 (1979) 19.
  27. X. Q. Li, R. J. Zhao, Y. Wang, X. Y. Sun, W. Sun, C. Z. Zhao and K. Jiao, *Electrochim. Acta*, 55 (2010) 2173.
  28. H. Xie, G. L. Luo, Y. Y. Niu, W. J. Weng, Y. X. Zhao, Z.Q. Ling, C. X. Ruan, G. J. Li and W. Sun, *Mat. Sci. Eng. C-Mater.*, 107 (2020) 110209.
  29. W. S. Zhao, X. Y. Li, Z. R. Wen, X. L. Niu, Q. F. Shen, Z. L. Sun, R. X. Dong and W. Sun, *Int. J. Electrochem. Sci.*, 12 (2017) 4025.
  30. W. Sun, L. F. Li, B. X. Lei, T. T. Li, X. Z. Ju, X. Z. Wang and Z. F. Sun, *Mat. Sci. Eng. C-Mater.*, 33 (2013) 1907.
  31. X. Q. Liu, L. H. Shi, W. X. Niu, H. J. Li and G. B. Xu, *Biosens. Bioelectron.*, (2008) 1887.
  32. Y. Y. Niu, R.Y. Zou, H. A. Yones, X. B. Li, X. L. Niu, Y. Chen, P. Li, and W. Sun, *J. Chin. Chem. Soc.*, 65 (2018) 1127.
  33. T. R. Zhan, X. J. Wang, X. J. Li, Y. Song and W. G. Hou, *Sensor. Actuat. B-Chem.*, 228 (2016) 101.